Tortuosity and anomalous diffusion in the neuromuscular junction

Daniel J. Lacks
Department of Chemical Engineering, Case Western Reserve University, Cleveland, Ohio 44106, USA
(Received 10 December 2007; revised manuscript received 4 February 2008; published 17 April 2008)

The signal transfer from nerve to muscle occurs by diffusion across the neuromuscular junction. The continuum level analysis of diffusion processes is based on the diffusion equation, which in one dimension is $\partial c/\partial t = D(\partial^2 c/\partial x^2)$, where c is the molecular concentration and D is the diffusivity. However, in confined systems such as the neuromuscular junction, the diffusion equation may not be valid, and even if valid the value of D may be altered by the confinement. In this paper, Monte Carlo simulations are used to probe diffusion at the molecular level in a realistic model of a neuromuscular junction. The results show that diffusion is anomalous (i.e., not described by the diffusion equation) for time scales less than ~0.01 s, which is the time scale relevant for signaling processes in the synapse. At longer time scales, the diffusion is normal (i.e., described by the diffusion equation), but with a value of D that is reduced by a factor of ~5 times compared to the value for diffusion in open space. As the width of the synaptic cleft decreases, these effects become even more pronounced. The physical basis of these results is described in terms of the structure of the neuromuscular junction.

DOI: 10.1103/PhysRevE.77.041912 PACS number(s): 87.16.dp, 87.16.af, 87.19.lg

I. INTRODUCTION

The diffusion of molecules in confined spaces plays important roles in many biological processes. As examples, the signaling for muscle action from a nerve is mediated by the diffusion of acetylcholine from a nerve cell to a muscle cell across the neuromuscular junction, and drug delivery in the brain occurs by diffusion in the brain extracellular space. Both the neuromuscular junction and the brain extracellular space are characterized by channels with widths of less than 50 nm, and contorted and branching paths.

It is well known that these confining environments reduce the effective diffusivity of a molecule in comparison to its diffusivity in open space [1–3]. These effects are of interest because diseases can alter the size and geometry of the confining environments, and the resulting change in diffusivity may underlie disease symptoms [4–8]. For example, a recent study suggests that Alzheimer's disease may be related to changes in diffusivity in the extracellular space of the brain [9]. This reduction in diffusivity is often characterized by the effective tortuosity $\lambda = (D_0/D)^{1/2}$, where D_0 is the diffusivity in open space and D is the diffusivity in the confining environment; in the brain extracellular space, experiments show that $\lambda \sim 1.6-2.1$ [1,3]. The decrease in diffusivity can come about in a number of ways: Contorted paths make molecules travel roundabout routes to get to a destination [10], dead-end spaces effectively trap molecules to delay their net movement [11–13], and interactions with the walls of the confining environment or extracellular macromolecules slow the movement of the molecules [14–16].

Analysis of diffusion at the continuum level usually proceeds via the diffusion equation, which in one dimension is

$$\frac{\partial c(x,t)}{\partial t} = D\frac{\partial^2 c(x,t)}{\partial x^2}, \tag{1}$$

where $c(x,t)$ is the concentration as a function of position x and time t. For example, the solutions of this equation are used to extract values of the diffusivity from experiments of diffusion in the brain extracellular space [1,3]. Also, this equation is used in modeling studies of the neuromuscular junction [17–19].

However, the diffusion equation is not universally valid [20–22]. The validity of the diffusion equation can be assessed by checking the validity of one of its solutions: For molecules released from a point source at time $t=0$, the mean-squared displacement of the molecules, $\langle x^2 \rangle$, grows with time as

$$\langle x^2 \rangle = 2Dt. \tag{2}$$

When this relation does not hold, the diffusion equation is not valid and "anomalous" diffusion occurs. The nature of the anomalous diffusion is characterized either by the scaling exponent α,

$$\langle x^2 \rangle = 2Dt^{\alpha}, \tag{3}$$

or by an apparent diffusivity that changes with the time scale of the observation,

$$D_{\text{app}}(t) = \langle x^2 \rangle/(2t). \tag{4}$$

The origins of anomalous diffusion can be understood in terms of a random walk that proceeds by steps of variable size separated by waiting times of variable duration. If the average step size L and average waiting time between steps τ are well defined, then diffusion is normal with $D = L^2/(2\tau)$. However, τ is not well defined and diffusion is anomalous with $\alpha < 1$ if the distribution of waiting times is broader than the observation time. If the waiting time distribution is finite (or decays sufficiently fast), then the anomalous diffusion is transient and normal diffusion occurs at long times; however, if the waiting time distribution is scale-free (e.g., a power-law distribution), then the diffusion is anomalous on all time scales. Experimental evidence for anomalous molecular diffusion has been found in systems similar to that investigated here: e.g., packed erythrocyte systems that serve as models for the brain extracellular space [23], and the dendrites of Purkinje cells [24].

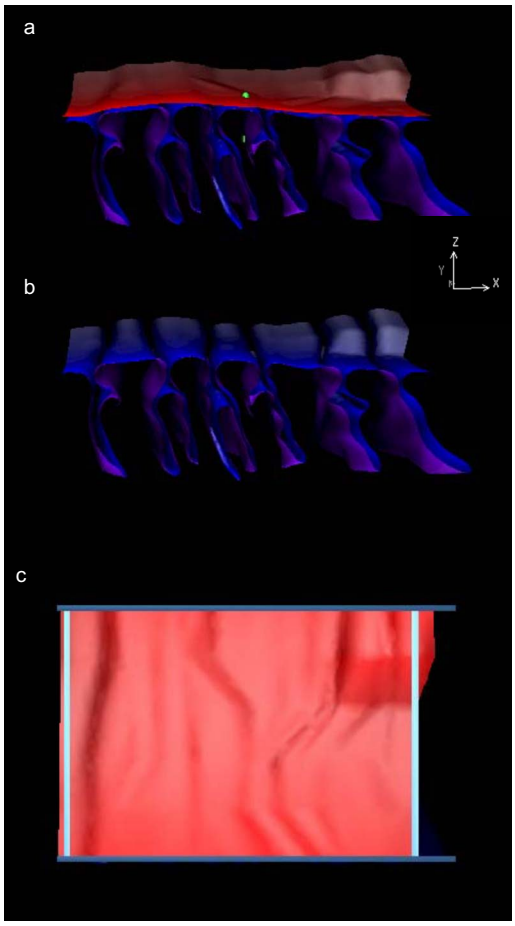

FIG. 1. (Color online) The neuromuscular junction model of Stiles *et al.* [25]. The upper (red) surface is the nerve membrane, and the lower (blue/violet) surface is the muscle membrane. (a) View from the side; spheres mark the molecule release sites, which are near the nerve membrane and within a junctional fold. (b) Same as (a), but with the nerve membrane removed for clarity. (c) View from above the nerve membrane, also showing the four walls added as part of the procedure to include periodic boundary conditions (see the text). These images were created with DREAMM version 3 [28,29].

The present investigation uses Monte Carlo simulations to determine how diffusion in the neuromuscular junction is affected by the confining environment. In particular, the effects of the confining environment on the effective tortuosity and the validity of the diffusion equation are studied. The simulations are carried out with a realistic model of a neuromuscular junction developed previously by Stiles *et al.* [25]; this approach thus differs from previous simulations of diffusion in extracellular spaces that addressed simplified *ad hoc* geometries [10,12,13,24,26].

II. COMPUTATIONAL METHODS

Molecular diffusion is analyzed in a realistic model of a neuromuscular junction, shown in Fig. 1. This model was derived by Stiles *et al.* from transmission electron microscopy images of a rat neuromuscular junction [25,27]. The width of the synaptic cleft that separates the nerve and muscle membranes varies in the range 0.015–0.050 μm (because the membranes are not flat). The junctional folds of the muscle membrane are oriented parallel to the y dimension, and have depths of $\sim$0.8 μm and widths of $\sim$0.1 μm. The overall size of the model is $\sim$2.7 μm in the x dimension, and $\sim$2 μm in the y dimension.

The MCell program [28,29] (version 3) is used to carry out Monte Carlo simulations of the dynamic trajectories of probe molecules. The simulation treats molecules as distinct particles, with each molecule i characterized by its position at time t: $x_i(t)$, $y_i(t)$, $z_i(t)$. The molecular trajectory proceeds in discrete time steps δt. At each step, each molecule i is displaced by the amounts $\delta x_i, \delta y_i, \delta z_i$, where these values are chosen randomly from a Gaussian distribution with variance $2D_0\delta t$; with this procedure the molecules undergo diffusive motion in open space described by the diffusivity D_0. When these displacements bring a molecule into contact with a membrane, the molecule is reflected from the membrane.

Due to the small size of the model (2–3 μm in the lateral dimensions), molecules would exit the system after short times (<0.5 ms), which precludes analysis of diffusion on experimentally relevant time scales. To circumvent this problem, periodic boundary conditions are implemented in the lateral dimensions; this procedure is standardly used in molecular simulations, to avoid surface effects [30]. As shown schematically in Fig. 2(a), the unit that is repeated periodically consists of four "primitive cells" (a primitive cell is the model in Fig. 1), with orientations such that adjacent cells are mirror images of each other (for reasons explained below).

While the MCell program does not include an option for periodic boundary conditions, the effects of periodic boundary conditions can nevertheless be implemented with the following method. This method allows the dynamics through the extended periodic system [Fig. 2(a)] to be addressed by explicitly modeling only the dynamics in a single primitive cell [the shaded cell in Fig. 2(a), denoted the "home cell"]. To implement this method, solid (reflecting) walls are included near the lateral edges of the system, as shown in Fig. 1(c). When a molecule hits one of these walls, it is reflected back into the home cell, but its identity changes in a way that signifies that the molecule would have proceeded to the next primitive cell if the wall were not there. This procedure is shown in Fig. 2(b): When a molecule in the home cell, $A(0)$, collides with the wall at $+x$ its identity changes to $A(+1)$, because it would have moved to the first primitive cell to the right of the home cell if the wall were not present. The $A(+1)$ molecule changes back to an $A(0)$ molecule if it hits the $+x$ wall, but changes to an $A(+2)$ molecule if it hits the $-x$ wall. Similarly, the $A(+2)$ molecule changes back to an $A(+1)$ molecule if it hits the $-x$ wall, but changes to an $A(+3)$ molecule if it hits the $+x$ wall. This trajectory shown in Fig. 2(b) thus mimics the green-line (right-pointing) trajectory in the extended periodic system of Fig. 2(a); the index n in the notation $A(n)$ represents the number of primitive cells the molecule has traversed. For a molecule moving in the opposite direction, the trajectory shown in Fig. 2(c) similarly mimics the red-line (left-pointing) trajectory in Fig. 2(a). From the position of a molecule in the home cell and its

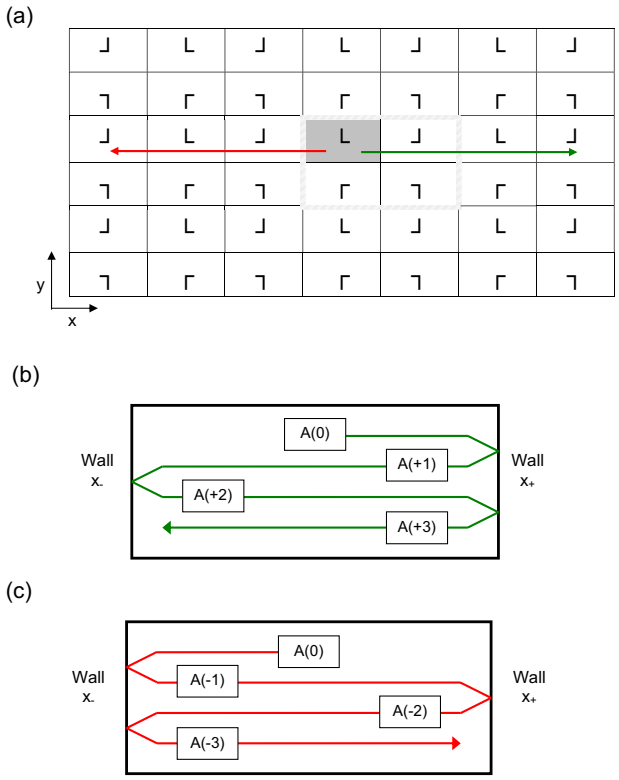

FIG. 2. (Color online) Periodic boundary implementation. (a) Extended system with periodic images. Each rectangle represents a "primitive cell" corresponding to the neuromuscular junction model of Stiles *et al.* [25]. The symbol inside each rectangle describes the orientation of the primitive cell. The periodically repeating unit is outlined, and consists of four primitive cells. Diffusion throughout this extended system is analyzed, even though molecules are explicitly modeled only in the "home cell," shown as shaded. (b) Trajectory in the home cell corresponding to a molecule moving in the positive x direction in the extended periodic system [green (right-pointing) line in part (a)]. Note that the identity of the molecule changes each time it reflects from a wall, with the index n, in notation $A(n)$, describing the number of primitive cells moved through in the extended periodic system. (c) Trajectory in the home cell corresponding to a molecule moving in the negative x direction in the extended periodic system [red (left-pointing) line in part (a)].

index n, the position of the molecule in the extended periodic system [Fig. 2(a)] can be determined. The changes of identity of the molecules when they hit walls are incorporated in MCell as chemical reactions (with large rate constants), as listed in Table I.

The structural anisotropy of the neuromuscular junction causes diffusion to be anisotropic, with the diffusivity being different along the three dimensions. Since the x dimension exhibits the interesting structural features that impact diffusion, the focus of this study is specifically the dynamics along this dimension, characterized by the mean-squared displacements obtained as

$$\langle x^2 \rangle = \frac{1}{N} \sum_{i=1}^{N} [x_i(t) - x_i(0)]^2. \tag{5}$$

The values of $x_i(t)$ are obtained from the positions of the particles within the home cell at time t (which are extracted from data files created by MCell), and the identity of the particles (which determines the primitive cell that the particle would be in, with the periodic boundary conditions). While in principle periodic boundary conditions are used in the x and y dimensions, in practice the periodicity in the y dimension is ignored here because the diffusive behavior in this direction is not addressed.

The trajectories are determined for $N=10\,000$ molecules with $D_0=0.6\ \mu\text{m}^2/\text{ms}$, the value for acetylcholine [31]. A simulation time step of $\delta t=1.67\times10^{-4}$ ms is used in most simulations; to test the effect of the magnitude of the time step, a simulation is also run with $\delta t=1.67\times10^{-5}$ ms. All molecules are released from a single location, which is either near the nerve membrane or within a junctional fold [see Fig. 1(a)]. The simulations are carried out for up to 20 million Monte Carlo steps (times over 3 s). All simulations are run on an Intel Core2 computer (2.66 GHz), for which 200 000 Monte Carlo steps take approximately one hour in real time.

III. RESULTS

A. Molecule release site near nerve membrane

Molecule release near the nerve membrane mimics the physiological process in which acetylcholine molecules are released from vesicles at the surface of the nerve membrane. A snapshot of the system at time $t=33$ ms is shown in Fig. 3; the different colors represent molecules that would be in different primitive cells of the extended periodic system [see Fig. 2(a)].

The results for $\langle x^2 \rangle$ as a function of time are shown in Fig. 4(a). The log-log plot emphasizes the scaling of $\langle x^2 \rangle$ and t: For normal diffusion, where $\langle x^2 \rangle = 2Dt$, the data appear linear on the log-log plot with a slope of 1 and a y intercept (at $t=t_x$) of $2Dt_x$. Three time scale regimes are evident in Fig. 4(a):

TABLE I. "Chemical reactions" included in the MCell simulation in order to implement periodic boundary conditions (see Fig. 2 and the text for more details).

At wall W_-		At wall W_+	
Forward	Reverse	Forward	Reverse
$A(0) @ W_- \rightarrow A(-1)$	$A(-1) @ W_- \rightarrow A(0)$	$A(0) @ W_+ \rightarrow A(+1)$	$A(+1) @ W_+ \rightarrow A(0)$
$A(+1) @ W_- \rightarrow A(+2)$	$A(+2) @ W_- \rightarrow A(+1)$	$A(-1) @ W_+ \rightarrow A(-2)$	$A(-2) @ W_+ \rightarrow A(-1)$
$A(-2) @ W_- \rightarrow A(-3)$	$A(-3) @ W_- \rightarrow A(-2)$	$A(+2) @ W_+ \rightarrow A(+3)$	$A(+3) @ W_+ \rightarrow A(+2)$
…	…	…	…

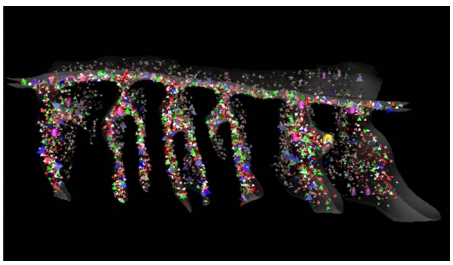

FIG. 3. (Color online) Snapshot of the system after the time $t=33$ ms. The different colors represent molecules that would be in different primitive cells of the extended periodic system [Fig. 2(a)], as follows. White: $n=0$; red: $n=\pm 1$; green: $n=\pm 2$; blue: $n=\pm 3$; purple: $n=\pm 4$; yellow: $n=\pm 5$; where n is the number of primitive cells away from the home cell. Note that the sizes of the molecules are arbitrary, and the less numerous types (e.g., $n=\pm 3$; $n=\pm 4$) are shown larger for emphasis. This image was created with DREAMM version 3 [28,29].

(i) At short times ($t<\sim 0.05$ ms), the simulation results follow a line with a slope of 1 and y intercept corresponding to D_0. Thus the molecules undergo normal diffusion with their characteristic diffusivity $D_0=0.6\ \mu\text{m}^2/\text{ms}$, as they would in the absence of any confining environment. This occurs because the nerve membrane is relatively flat and thus does not affect diffusion (along the x dimension), and the molecules have not yet approached the junctional folds of the muscle membrane. At times of ~ 0.05 ms, the molecules begin entering the junctional folds, which impedes their movement along the x direction and causes the deviation from linearity in Fig. 4(a).

(ii) At long times ($t>\sim 5$ ms), the simulation results again follow a line with a slope of 1, but with a smaller y intercept. In this time scale regime, normal diffusion occurs but with the lower diffusion constant $D=0.12\ \mu\text{m}^2/\text{ms}$, which corresponds to an effective tortuosity $\lambda=2.2$. To elucidate this result, it is noted that most of the molecules are located within the junctional folds, and very few are in the spaces between folds (see Fig. 3)—i.e., the molecules are trapped in junctional folds, and diffusion occurs by hopping between adjacent junctional folds. The waiting time distribution for molecules to hop between adjacent junctional folds is determined by releasing molecules within a junctional fold [see Fig. 1(a)], and then considering a molecule to be "escaped" when it has passed through one of two planes midway between the junctional fold of origin and the adjacent junctional folds. Figure 5(a) shows the fraction of the molecules remaining in the junctional fold of origin, as a function of time: While there is a wide distribution of escape times, the average escape time is 0.7 ms, and virtually all molecules have escaped by ~ 5 ms. Thus, for time scales greater than ~ 5 ms, the molecule undergoes normal diffusion by a one dimensional random walk between junctional folds. Taking the average step size $L=0.45\ \mu\text{m}$ (the average distance between adjacent junctional folds), and the average waiting time $\tau=0.7$ ms (the average escape time), the diffusivity is estimated from the random walk model as $D=L^2/2\tau=0.14\ \mu\text{m}^2/\text{ms}$. This estimate compares well with the simulation result described above.

(iii) For intermediate times ($\sim 0.05\ \text{ms}<t<\sim 5$ ms), the mean-squared displacements do *not* scale linearly with time, and instead $\langle x^2\rangle=2Dt^\alpha$, where $\alpha\sim 0.7$. Thus, anomalous diffusion occurs in this time scale regime. The reason for the anomalous diffusion is evident from Fig. 5(b): The average escape time from a junctional fold is only a well-defined value for observation times greater than ~ 5 ms, and so the random walk of molecules between junctional folds (described above) does not have a well-defined value of the waiting time between steps for times less than 5 ms.

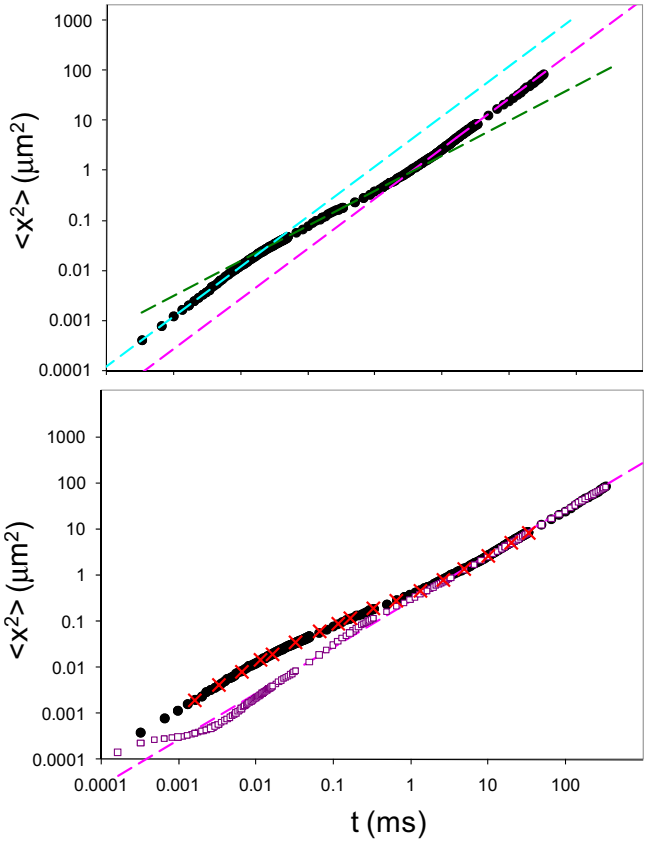

FIG. 4. (Color online) Results for mean-squared displacement as a function of time. (a) Molecules released near nerve membrane. (b) Comparison of results for molecules released within junctional fold (open squares) with molecules released near the nerve membrane (filled circles); the crosses represent values obtained with the smaller time step $\delta t=1.67\times 10^{-5}$ ms. The dashed blue (upper) line describes normal diffusion (i.e., slope of 1) with a diffusivity $D=D_0$, the dashed pink (lower) line represents normal diffusion with diffusivity $D=0.12\ \mu\text{m}^2/\text{ms}$, and the dashed green line (with different slope) represents anomalous diffusion with an exponent $\alpha=0.7$.

The results appear to be converged with respect to the magnitude of the time step used in the simulation, as shown in Fig. 4(b)—i.e., the results are indistinguishable when the simulations are carried out with a time step that is smaller by a factor of 10.

B. Effects of position of molecule release site

In Fig. 4(b), the mean-squared displacements are compared for molecules released from different sites (near the

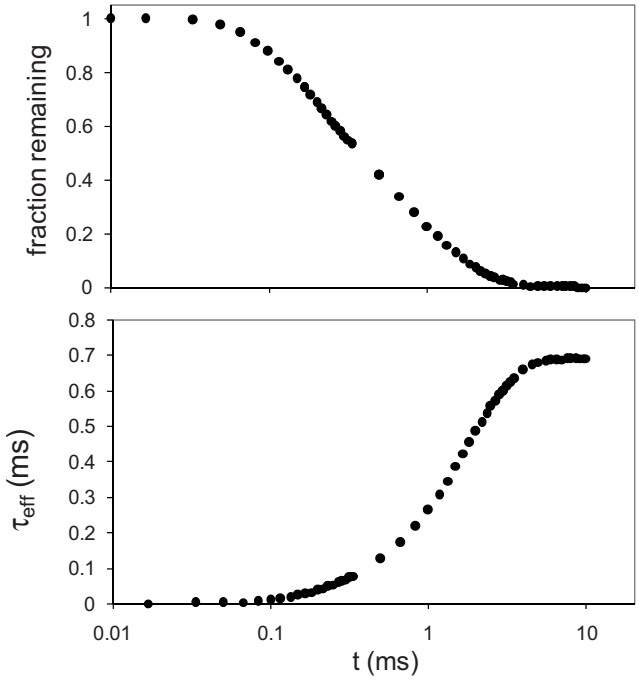

FIG. 5. Escape of molecules from a junctional fold. (a) Fraction of molecules remaining in fold as a function of time. (b) Running calculation of average escape time, $\tau_{\text{eff}}(t)=\int_0^t P_{\text{esc}}(t')t'dt'$, where $P_{\text{esc}}(t')$ is the probability that a molecule escapes at time t'. For $t\rightarrow\infty$, τ_{eff} is the average escape time.

nerve membrane and inside a junctional fold). At long times ($t>\sim 5$ ms), the results from the two release sites are very similar. However, for shorter times ($t<\sim 5$ ms), the results depend strongly on the position of the release site. In this time scale regime, the scaling of $\langle x^2\rangle$ is generally not linear with t, implying that the diffusion is generally anomalous. Also, the magnitude of the apparent diffusivity $D_{\text{app}}(t)=\langle x^2\rangle/(2t)$ depends on the release site; e.g., at $t=0.1$ ms, the apparent diffusivity for the two sets of results differs by almost a factor of 3.

C. Effects of width of the synaptic cleft

Simulations are carried out with the position of the nerve membrane shifted away from the muscle membrane by the amount Δs; simulations are carried out with $\Delta s>0$ and $\Delta s<0$, corresponding to increases and decreases of the width of the synaptic cleft. These simulations are run with the molecules released from within a junctional fold, and the results for the mean-squared displacements are shown in Fig. 6. For times $t<\sim 0.05$ ms, the results are independent of the value of Δs, because molecules have not exited the junctional fold in this time and thus are not affected by the position of the nerve membrane. At intermediate times the diffusion is anomalous and strongly dependent on Δs, and at long times normal diffusion occurs with a diffusivity that depends on the magnitude of Δs (except for the smallest nerve-muscle separation examined, which is addressed in more detail below).

The diffusivity in the long-time limit is strongly affected by the width of the synaptic cleft. For $\Delta s=1$ μm, the long-time diffusivity is very close to D_0 ($\lambda=1.07$), because most molecules are located outside of the junctional folds, and thus move through open space without impedance from the junctional folds. As the separation becomes small, most molecules are trapped within the junctional folds, and diffusion occurs as a random walk between adjacent junctional folds. As Δs decreases, it is more difficult for a molecule to escape from a junctional fold, because the escape route is a narrow slit that gets even narrower as Δs decreases. Thus, as Δs decreases, the average waiting time τ for steps between adjacent junctional folds increases, which makes the diffusivity $D=L^2/(2\tau)$ smaller. For this reason the effective tortuosity in the long-time limit, shown in Fig. 7, increases strongly with decreasing separation.

Before the normal diffusion regime is reached, the diffusion is anomalous. The transition to normal diffusion is shifted to longer times as the synaptic cleft becomes narrower. This shift is understood in terms of the picture of diffusion as a random walk between adjacent junctional folds: as Δs decreases, the waiting time distribution for steps

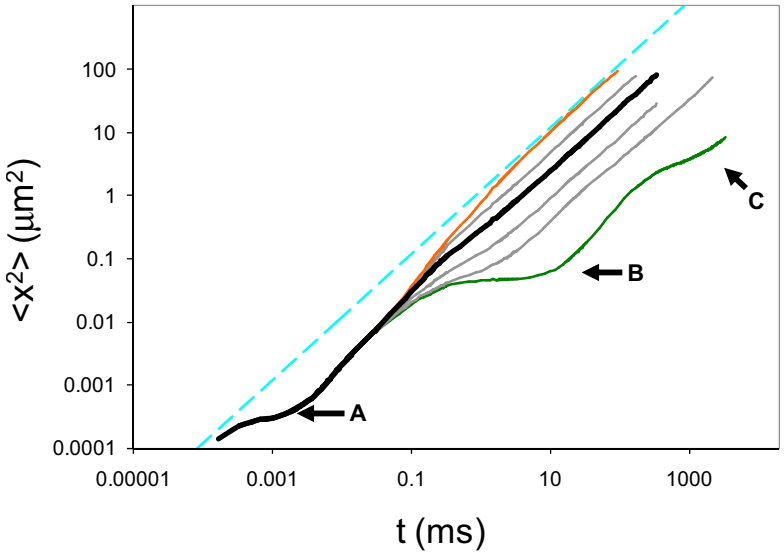

FIG. 6. (Color online) Results for the mean-squared displacement as a function of time, as the separation between the nerve membrane and the muscle membrane is shifted by Δs. The curves, from top to bottom, represent results with $\Delta s=1.0$ μm, $\Delta s=0.05$ μm, $\Delta s=0$, $\Delta s=-0.02$ μm, $\Delta s=-0.025$ μm, and $\Delta s=-0.03$ μm.

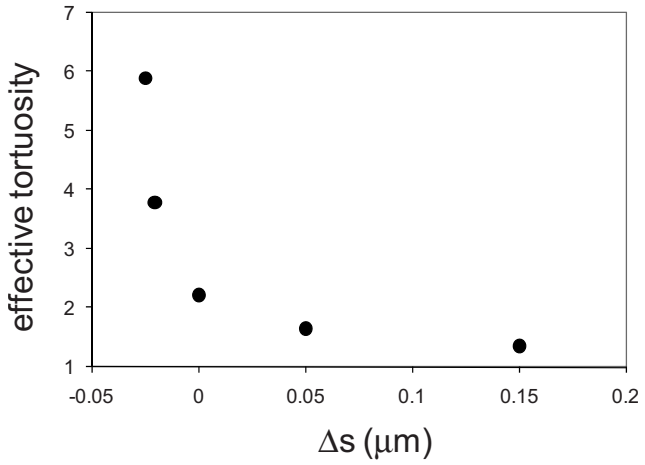

FIG. 7. Effective tortuosity in the long-time limit, as the separation between the nerve membrane and the muscle membrane is shifted by Δs.

becomes broader (as described above), and the diffusion is anomalous when the observation time is smaller than the breadth of the waiting time distribution (such that an average waiting time is not well defined).

The simulation with $\Delta s = -0.03$ μm did not reach the normal diffusion regime within a 3.3 s simulation (20 000 000 time steps). The mean-squared displacement results for this system shows plateaus that are evidence of a hierarchy of traps that hinder diffusion on different length and time scales. On time scales of ~ 0.001 ms (plateau A), the molecules are trapped within a pocket of the junctional fold, with length scale ~ 0.02 μm (length scale given by $\langle x^2 \rangle^{1/2}$). On time scales of $\sim 1-10$ ms (plateau B), the molecules are trapped within the junctional folds, with length scale ~ 0.2 μm (note this is greater than the width of the junctional fold, due to the slanted orientation of the folds). On time scales of ~ 1000 ms (plateau C), the molecules are trapped with a length scale of ~ 2 μm. The origin of this trap is as follows: The nerve membrane and top of the muscle membrane are bumpy rather than flat, and as Δs decreases the two surfaces come in contact at some points but not at others; the points of contact are shown in blu (darker) e in Fig. 8. The passage of molecules is blocked when there is contact of the nerve and muscle membranes, and for $\Delta s \sim -0.0307$ μm there is complete blockage between two adjacent junctional folds; at this point diffusion throughout the extended periodic system [Fig. 2(a)] is not possible. At $\Delta s = -0.03$ μm, the blockage is incomplete and there is a small opening that allows passage between the adjacent junctional folds, but this region acts to trap molecules until their random motion brings them through the opening. The length scale of this trap (~ 2 μm) represents the distance between this trap and its periodic images in the extended periodic system. In this time scale regime (~ 1000 ms), diffusion occurs as a random walk with $L \sim 2$ μm and a waiting time τ corresponding to the average time for a molecule to escape through this small opening.

IV. DISCUSSION AND CONCLUSIONS

Simulations are carried out to address how the confining environment of the neuromuscular junction affects molecular

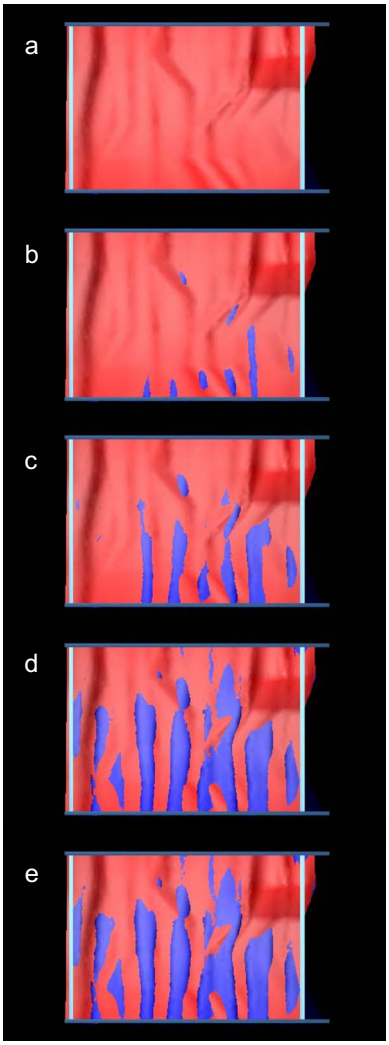

FIG. 8. (Color online) View of neuromuscular junction from above the nerve membrane, as the separation between the nerve membrane and the muscle membrane is shifted by Δs. The blue (darker) color represents points where the two membranes overlap, such that the space between the membranes is pinched off. (a) $\Delta s = 0$, (b) $\Delta s = -0.02$ μm, (c) $\Delta s = -0.025$ μm, (d) $\Delta s = -0.03$ μm, and (e) $\Delta s = -0.0307$ μm. These images were created with DREAMM version 3 [28,29].

diffusion. By using a realistic model for the neuromuscular junction, and a Monte Carlo method to treat molecules as distinct particles moving in space, the nature of the diffusion is determined in a way that is nonempirical and independent of assumptions. Diffusion in the neuromuscular junction is shown to be anomalous for time scales less than $\sim 1-10$ ms (depending on the value of D_0, as discussed below). This result is significant because this is the physiologically relevant time scale for many processes in the neuromuscular junction. Therefore, to accurately model these processes in the neuromuscular junction, methods that treat the molecules at a particle level rather than a continuum level are necessary.

While the results are shown here for molecules with $D_0 = 0.6$ μm^2/ms, the behavior of molecules with other values of D_0 can be derived as follows. The value of D_0 enters the

simulation in that the Monte Carlo step sizes are chosen randomly from a Gaussian distribution with variance $2D_0\delta t$. Since it is the product $D_0\delta t$ that is relevant, changing D_0 by the factor f while changing δt by a factor $1/f$ would give identical results. For example, the mean-squared displacements for molecules with $D_0=0.3\ \mu m^2/ms$ would differ from those for molecules with $D_0=0.6\ \mu m^2/ms$ only in that the time scale is larger by a factor of 2; e.g., for molecules with $D_0=0.3\ \mu m^2/ms$, diffusion is anomalous for timescales less than ~ 10 ms.

We point out that the present investigation does not attempt to realistically address the spatiotemporal distributions of molecules in the neuromuscular junction. This investigation focuses on the geometric factors that affect diffusion in the neuromuscular junction, but other factors will also affect the spatiotemporal molecular distributions within the junction. First, interactions with the extracellular matrix will further slow diffusion, as described above; previous work suggests that for acetylcholine, a smaller $D_0=0.3\ \mu m^2/ms$ would account for these effects [32], and the present results can be considered in terms of this value of D_0 as described in the paragraph above. Second, acetylcholine molecules bind reversibly to receptor sites, which thus act as traps that also hinder diffusion; depending on the concentrations of receptor sites and their effective trapping times, this effect could dominate the geometric effects described here. Third, chemical reactions will significantly alter the spatiotemporal molecular distributions; most importantly, acetylcholine is broken down by acetylcholine esterase. Note that while these latter two effects are important for acetylcholine, they are not as important for other species that diffuse in the neuromuscular junction, such as choline and potassium and sodium ions.

Changes in the width of the synaptic cleft alter the diffusion in the neuromuscular junction. In particular, decreasing the width causes a sharp increase in the tortuosity, while increasing the width causes a decrease in tortuosity that is much more gradual (Fig. 7). These changes are similar to those found in experiments of diffusion in the brain extracellular space, where the tortuosity increases with decreasing volume of extracellular space, but changes little with increasing volume of extracellular space [33]. This similarity suggests that physical origins of the tortuosity are similar in the two cases (trapping in dead-end spaces); simulations on simple model geometries with dead-end spaces have also shown this effect [13]. Recent work suggests that the natural width of a synaptic cleft represents an optimum that balances two competing effects: a narrower cleft allows a higher concentration of neurotransmitter in the synapse, but increases the electrical resistance [34]. The results shown here suggest that the influence of the width on diffusion could also play a key role in the determination of the optimum synaptic cleft width.

ACKNOWLEDGMENTS

This material is based on work supported by the National Science Foundation (Grant No. DMR-0402867). Assistance with the MCell program from Joel Stiles and Markus Dittrich is gratefully acknowledged.

[1] C. Nicholson, Rep. Prog. Phys. **64**, 815 (2001).
[2] D. K. Binder, M. C. Papadopoulos, P. M. Haggie, and A. S. Verkman, J. Neurosci. **24**, 8049 (2004).
[3] M. Stroh, W. R. Zipfel, R. M. Williams, W. W. Webb, and W. M. Saltzman, Biophys. J. **85**, 581 (2003).
[4] K. C. Chen and C. Nicholson, Proc. Natl. Acad. Sci. U.S.A. **97**, 8306 (2000).
[5] S. Hrabetova and C. Nicholson, J. Cereb. Blood Flow Metab. **20**, 1306 (2000).
[6] S. Hrabetova, J. Hrabe, and C. Nicholson, J. Neurosci. **23**, 8351 (2003).
[7] M. F. Lythgoe, D. L. Thomas, M. D. King, G. S. Pell, L. van der Weerd, R. J. Ordidge, and D. G. Gadian, Magn. Reson. Med. **53**, 593 (2005).
[8] I. W. Tatum, A. Malek, M. Recio, J. Orlowski, and R. Murtagh, Epilepsy Behav. **5**, 411 (2004).
[9] E. Sykova, I. Vorisek, T. Antonova, T. Mazel, M. Meyer-Luehmann, M. Jucker, M. Hajek, M. Ort, and J. Bures, Proc. Natl. Acad. Sci. U.S.A. **102**, 479 (2005).
[10] L. Tao and C. Nicholson, J. Theor. Biol. **229**, 59 (2004).
[11] S. Hrabetova and C. Nicholson, Neurochem. Int. **45**, 467 (2004).
[12] J. Hrabe, S. Hrabetova, and K. Segeth, Biophys. J. **87**, 1606 (2004).
[13] A. Tao, L. Tao, and C. Nicholson, J. Theor. Biol. **234**, 525 (2005).
[14] D. A. Rusakov and D. M. Kullmann, Proc. Natl. Acad. Sci. U.S.A. **95**, 8975 (1998).
[15] M. C. Papadopoulos, J. K. Kim, and A. S. Verkman, Biophys. J. **89**, 3660 (2005).
[16] R. G. Thorne and C. Nicholson, Proc. Natl. Acad. Sci. U.S.A. **103**, 5567 (2006).
[17] J. L. Smart and J. A. McCammon, Biophys. J. **75**, 1679 (1998).
[18] K. Tai, S. D. Bond, H. R. MacMillan, N. A. Baker, M. J. Holst, and J. A. McCammon, Biophys. J. **84**, 2234 (2003).
[19] Y. Cheng, J. K. Suen, Z. Radic, S. D. Bond, M. J. Holst, and J. A. McCammon, Biophys. Chem. **127**, 129 (2007).
[20] J. Klafter and I. M. Sokolov, Phys. World **18**, 29 (2005).
[21] R. Metzler and J. Klafter, J. Phys. A **37**, R161 (2004).
[22] M. J. Saxton, Biophys. J. **92**, 1178 (2007).
[23] L. L. Latour, K. Svoboda, P. P. Mitra, and C. H. Sotak, Proc. Natl. Acad. Sci. U.S.A. **91**, 1229 (1994).
[24] F. Santamaria, S. Wils, E. De Schutter, and G. J. Augustin, Neuron **52**, 635 (2006).
[25] J. R. Stiles, T. M. Bartol, M. M. Salpeter, E. E. Salpeter, and T. J. Sejnowski, in *Synapses*, edited by W. M. Cowan, T. C. Sudhof, and C. F. Stevens (Johns Hopkins University Press, Baltimore, 2001), pp. 681–731.
[26] L. P. Savtchencko and D. A. Rusakov, Neurochem. Int. **45**,

479 (2004).
[27] J. R. Stiles, Rat Neuromuscular Junction, http://www.mcell.psc.edu/tutorials/ratnmj.html(2006).
[28] J. R. Stiles, D. Van Helden, T. M. Bartol, Jr., E. E. Salpeter, and M. M. Salpeter, Proc. Natl. Acad. Sci. U.S.A. **93**, 5747 (1996).
[29] J. R. Stiles and T. M. Bartol, in *Computational Neuroscience: Realistic Modeling for Experimentalists*, edited by E. De Schutter (CRC Press, Boca Raton, 2001), pp. 87–127.
[30] M. P. Allen and D. J. Tildesley, *Computer Simulation of Liquids* (Clarendon, Oxford, 1989), p. 24.
[31] V. E. Dionne, Biophys. J. **16**, 705 (1976).
[32] J. R. Stiles, I. V. Kovyazina, E. E. Salpeter, and M. M. Salpeter, Biophys. J. **77**, 11777 (1999).
[33] J. Kume-Kick, T. Mazel, I. Vorisek, S. Hrabetova, L. Tao, and C. Nicholson, J. Physiol. (London) **542.2**, 515 (2002).
[34] L. P. Savtchenko and D. A. Rusakov, Proc. Natl. Acad. Sci. U.S.A. **104**, 1823 (2007).